

Article

An Empirical Study of ATCOR vs. FLAASH Atmospheric Correction for Hyperspectral Classification of Tree Species Using SVM

Morteza Shahriari Nia^{1,*}, Daisy Zhe Wang¹, Paul Gader¹, Stephanie Ann Bohlman³, and Milenko Petrovic²

¹ Department of Computer and Information Science and Engineering, University of Florida, 432 Newell Dr., Gainesville, Florida 32611; E-Mails: msnia@cise.ufl.edu; daisyw@cise.ufl.edu; pgader@cise.ufl.edu;

² Institute for Human and Machine Cognition, 15 SE Osceola Ave, Ocala, Florida 34471; E-Mail: mpetrovic@ihmc.us;

³ School of Forest Resources and Conservation, University of Florida, 349 Newins Ziegler Hall, Gainesville, Florida 32611; E-Mail: sbohlman@ufl.edu;

* Author to whom correspondence should be addressed; E-Mail: msnia@cise.ufl.edu.

Received: / Accepted: / Published:

Abstract: Identifying savannah species at ecological scale is a key step in measuring biomass, carbon reserves, drought and predictions on spreading of invasive species. In this paper we perform classification and geo-mapping of tree species from hyperspectral imagery collected using AVIRIS airborne sensors at pixel level. We provide a thorough comparison of the effects of ATCOR and FLAASH atmospheric corrections in prediction accuracy. We exploit Gaussian Filters to eliminate sensor measurements and calibration errors. To the best of our knowledge we are the first in employing Gaussian Filters for hyperspectral species classification. The area of study is Ordway-Swisher Biological Station in north-central Florida. Due to the structure of the collected field data, we realized that applying NDVI and NIR filters do not play constructive roles in classification. Species classification was performed using variety of Support Vector Machine kernels where Radial Basis outperformed others. Our classification produces accurate predictions of about 75%.

Keywords: Species classification; Atmospheric Corrections; FLAASH; ATCOR; Ordway-Swisher Biological Station; National Ecological Observatory Network;

1. Introduction

Mapping tree species by remote sensing techniques is an essential step in understanding how planetary species play role at ecological scale. This will enable us to study land covers, climate change, invasive species, plant competitions, field fire potentials and spreading routes, and soil characteristics among others [1,2]. This kind of research has only been possible via the technological advancements in *remote sensing* facilities such as hyperspectral imagery or Light Detection and Ranging (LiDAR).

Various studies have been dealing with identifying tree species both at pixel level and crown level. As technology becomes available and economically feasible, studies tend to cover larger areas and try to focus on more fine-grained details. Here we provide an overview beginning from high-level approaches to more fine-grained aspects of remote sensing of plant species using hyperspectral technologies. Carnegie Airborne Observatory¹ (CAO) is a major pioneer in employing airborne technology for remote sensing at ecology scale where they study large areas in Amazonians, Kruger National Park in South Africa, and Madagascar among others. Colgan et al. [1] uses a two stage Support Vector Machine (SVM) at pixel level and at crown level respectively for tree species classification where LiDAR measurements were used for crown segmentation. Féret and Asner [3] study the accuracy of various parametric/non-parametric supervised classification techniques and observed that there is a clear advantage in using Regularized Discriminant Analysis, Linear Discriminant Analysis, and SVM. There are other tree species classification efforts such as [3-9] that share the same approach with minor variations.

Cho et al. [3] goes deeper and compares the performance of different hyperspectral band ranges of CAO, WorldView2 and QuickBird for classification performance. By convolving the 72 bands of CAO to eight and four multispectral channels available in the WorldView-2 and QuickBird satellite sensors respectively, they observed that WorldView-2 produced more accurate classification results than QuickBird and finally CAO. Clark et al. looks more into signal sources and compares lab measurements to pixel and to crown level data and try to identify important wavelength regions for species discrimination. They observed that optimal regions of the spectrum for species discrimination varied with scale. However, near-infrared bands were consistently important regions across all scales. Bands in the visible region and shortwave infrared were more important at pixel and crown scales [10]. Clark et al. in another work evaluates the applicability of different parameters (indexes, derivatives, signals intensities) for classification [11].

As we go deeper into signal details, there are works on identifying more context specific features. Baldeck and Asner [12] try to measure how similar beta diversity of regions are; they use distance measures such as Euclidean distance and K-means clustering in unsupervised models. Using these clustering techniques one can provide a quick understanding of beta diversities; this avoids costly and time-consuming field data collections. However, this line of research needs more work as about 50% of pixels are classified as *other*, therefore any conclusion at this scale of uncertainty is not necessarily helpful, the same holds in Baldeck et al.'s latter work in [13]. Within the same line of research we

¹ <http://cao.stanford.edu/>

observe that different bands in a hyperspectral image have different signal to noise ratios. Principal Components (PC) transform will not always result in components with a steadily increasing noise level and this makes setting a cut-off point difficult in dimensionality reduction. Minimum Noise Fraction which is a modified PC transform produces a set of principal component images ordered in terms of decreasing signal quality [14].

Even lower in signal level we face the impact of atmosphere in collected signals. The impact of the atmosphere is variable in space and time and is usually considered as requiring correction for quantitative remote sensing applications [15–18]. There has been plenty of research investigating the effects of different atmospheric correction methods for Landsat [19,20], QuickBird [21], and many other imaging spectrometer data [22,23]. But unfortunately none of them addresses the impact of atmospheric correction for plant species classification. The main goal of such papers are usually bound to low level signal manipulation, estimation and at most comparison to simple ground data such as asphalt or gravel. The final goal of atmospheric correction, which in our context is species classification, is not a well-studied subject. There are several approaches at atmospheric correction, some include scene-derived adjustments, in which in-scene statistics are used, such as the Darkest Pixel method [21,24], or purely empirical methods where ground-recorded spectral data are required, e.g., the Empirical Line [25,26]. Some involve radiative transfer algorithms such as the 6S code [27] and MODTRAN [28], and others use in situ spectral data (model based) such as ATCOR (ATmospheric CORection) [29–32] and FLAASH (Fast Line-of-sight Atmospheric Analysis of Spectral Hypercubes) [33,34]. If ground data is not available radiative transfer models provide a cost and time effective solution, as for us such data is collected, we focus on ATCOR and FLAASH. Our results align with the performance by state-of-the-art comparison of the two as in [35], where they focused on basic endmember classification (asphalt, gravel, rocky areas, reddish soil, agricultural areas, grass/dry grass, mequis, and phrygana) but we look into the actual problem of tree species classification.

For our study we look into the data provided by National Ecological Observatory Network (NEON) for Ordway-Swisher Biological Station in north-central Florida, USA. Local ecological-site observations fall short on providing ecological-scale analysis of the environment. To solve this problem, NEON begins a 30-year ecology-monitoring project starting in 2016 with goals of discovering, understanding and forecasting parameters that impact climate change, land use change, invasive species, and etc at continental-scale. Needless to say that measurements and samples shall be collected using highly standardized methods and instrumentation so that data can be used intra-site. NEON will be monitoring sites within 20 eco-climatic domains across the contiguous United States, Alaska, Hawaii, and Puerto Rico coordinated with high resolution, regional airborne remote sensing observations [36]. It will also have 40 re-locatable terrestrial sites (mobile every five to seven years) as well as 36 aquatic sites¹. Airborne Observation Platform (AOP) is the remote sensing platform with equipment of meter/sub-meter resolution for hyperspectral and LiDAR measurements. This paper is a pilot study on the pre-mission airborne hyperspectral data collection. No operation at the scale and time span predicted to be fulfilled for NEON (neither geographical and timely span) has ever been carried out before [37].

¹ <http://www.neoninc.org/science/domains#sthash.aW1THj1N.dpuf>

The contributions of this paper are as follows: we perform plant species classification using SVM, we study the impact of different atmospheric correction techniques (ATCOR and FLAASH) for classification accuracy, and we propose to use Gaussian filters for de-noising reflectance values. Contrary to the general suggestion that removal of shady and non-green (low NDVI, low NIR) helps classification accuracy we show that in certain situations it is advised to preserve such pixel to enhance the aggregate performance of SVM. This can be helpful in finding maximum margin support vectors that avoids high bias in data (as opposed to high variance). The paper is organized as follows: Section 1 provides an introduction on the big picture of state-of-the-art remote sensing techniques for species classification and where we fit in. In Section 2 we discuss airborne data and field data collection details. Section 3 goes through the details of atmospheric correction details, Gaussian Filtering, low NDVI and low NIR pixels impacts, and also classification function details using SVM. In Section 4 we present our results and discuss the impacts of our contributions, finally we conclude in Section 5.

2. Data Collection

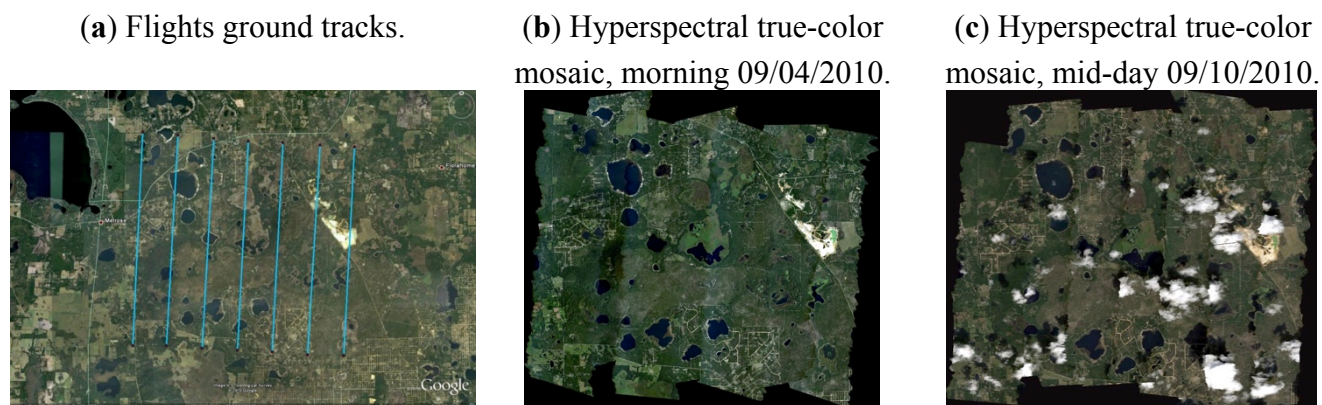
The NEON Southeast Domain 3 contains the southern portions of the Gulf Coast states, half of South Carolina, and all of Florida except for the southern tip. The candidate core site for Domain 3 is located at the Ordway-Swisher Biological Station (OSBS) which is an 37 km^2 area in Putnam County

Figure 1. Location of Ordway-Swisher Biological Station



in north-central Florida and is managed jointly by the University of Florida and the Nature Conservancy (Figure 1). OSBS features diverse natural forests, small pine plantations nearby, a range of wildlife species that reflects the area's ecological communities along with a 75-year history of low human impact. Nine major plant communities exist within the region (defined by the Florida Natural Areas Inventory) and these diverse targets are populated by sandhill, xeric hammock, upland mixed forest, baygalls, basin swamp, basin marsh, marsh lake, clastic upland lake and sandhill upland lakes. The sandhill community is managed using prescribed burning on a scheduled 3-year rotation. The ground sampling part of this campaign focused on a sandhill ecosystem dominated by Long-Leaf Pine (*Pinus Palustris*) and Turkey Oak (*Quercus Laevis*) [37,38].

Since the instrumentation slated for deployment on the eventual AOP remote sensing payloads were not yet available, airborne spectroscopic and LiDAR measurements were made during this campaign using existing systems that exhibit similar performance characteristics as the instrumentation under

Figure 2. JPL AVIRIS flights over OSBS [37]

development [38]. It is important to note that the actual system for NEON will have better conformance of hyperspectral/LiDAR integrations with better spatial resolution. However here we only focus on hyperspectral data.

AVIRIS (Airborne Visible/Infrared Imaging Spectrometer) operated by the Jet Propulsion Laboratory (JPL) deployed on a Twin Otter DeHavilland DHC-6-300 aircraft in partnership with the National Aeronautics and Space Administration Terrestrial Ecology Program was used to collect data. JPL has flown on two separate days over OSBS: morning of September 4, 2010 and mid-day of September 10, 2010. Both of the flights were flown at approximately 4000m AGL at approximately 90 knots with zenith angle of 180.0 and azimuth angle of 0.0 with Altitude of 13kft (SOG ~ 65-91kts)¹ at mostly clear with some haze for Sept. 4th and some puffy clouds for Sept. 10th. Details of these flights can be seen in Figure 2. Dependent on flight line, pixel size ranges from 3.3m to 3.6m. Hyperspectral data was atmospherically corrected using FLAASH and ATCOR algorithms. There are altogether 8 flight lines and 224 bands recorded with wavelengths from 365.93 nm to 2496.24 nm.

Atmospheric characterization relied on measurements of a CIMEL sun photometer in coordination with the NASA Aerosol Robotic Network². Measurements were collected on September 4, 2010 and the derived atmospheric information was used to improve the atmospheric correction of the AVIRIS spectrometer data. Detailed measurements such as aerosol optical thickness, water vapor, and etc are available online³. NEON personnel perform the ortho-rectification and atmospheric correction of the reflectance/radiance values.

2.1. Field Data

Geo-identifying of tree species as field data was collected on February 28th, 2014. A laptop preloaded with ArcMap and ENVI software was used in conjunction with a professional grade GPS.

¹ NASA JPL AVIRIS flight details:

http://aviris.jpl.nasa.gov/cgi/flights_10.cgi?step=view_flightlog&flight_id=f100904t01

http://aviris.jpl.nasa.gov/cgi/flights_10.cgi?step=view_flightlog&flight_id=f100910t01

² NASA AERONET: http://aeronet.gsfc.nasa.gov/cgi-bin/bamgommas_interactive

³ OSBS Aero Measurements: http://aeronet.gsfc.nasa.gov/cgi-bin/type_one_station_opera_v2_new?site=Ordway-Swisher

ArcMap reads GPS coordinates and maps identified canopy polygons in ENVI, which is pre-loaded with relevant flight data. In this way, we marked several geo-polygons that had similar plant species in ENVI. Later on we overlaid the identified polygons with proper JPL AVIRIS flight, which had the least amount of clouds. This approach works fairly well if you are not in a dense forest such as tropical forests where GPS signal under the tree canopy has high deviations due to NLOS (no-line of sight) of GPS signals. One should note that even with these considerations, commercial GPS have sub-meter accuracy and when combined with error accumulated in ortho-rectification of flight images we still need to mark several land marks such as roads, large trees or other land marks to be able to re-verify marked points in the map and avoid shifts in coordinates. Altogether we identified species for 1269 pixels. In Table 1 you can find the details of identified Regions of Interest (ROIs) along with their details. The closer ROI Ids are collected from closer vicinity (geographically/temporally), and the more distant ROI Ids means that canopies are more apart. You can see that some species are abundant (e.g. 334 for Turkey Oak) where others are less so (e.g. 81 for Laurel Oak). This bias in population size inadvertently affects classification accuracy. Figure 3 depicts the abundance of each canopy respectively. The Oak (other) species represent generic oak specie (*specie details unknown*). Live Oak is specifically Sand Live Oak (*Quercus Geminata*), Laurel Oak represents *Quercus Hemisphaerica*, Turkey Oak is *Quercus Laevis*, Longleaf Pine is *Pinus Palustris*, and Pine (other) represents a mixture of different varieties of pines: Longleaf Pine (*Pinus Palustris*), Loblolly Pine (*Pinus Taeda*) or Slash Pine (*Pinus Elliotti*).

3. Species Classification

Due to the large size of each pixel (3+ by 3+ square meters) we do not get pure pine or oak signals and there are lots of linear/nonlinear mixture of endmembers in each pixel (e.g. road, shadow, branch, under-score vegetation, multiple tree species and etc.). The timing of flights (September) adds to the challenge: leafs might not be as green or some trees might have already started to lose leaves and potentially leads to getting more branch or dead leaf signals. One should note that the more leaves a tree has and the greener the leaves are we will have better signal absorption in green/visible bands which are not present in dead leaves, branches or soil.

Figure 3. Field Data Distribution of ROIs.

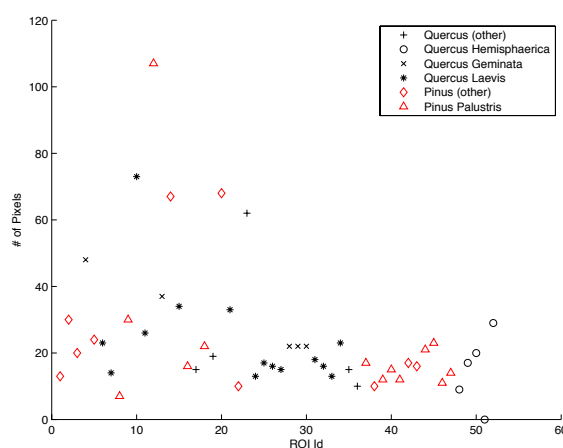


Table 1. Field Data Specifications

Specie	Broadleaf								Conifer			
	Oak (other)		Laurel Oak		Live Oak		Turkey Oak		Pine (other)		Longleaf Pine	
	ROI Id	Pixels	ROI Id	Pixels	ROI Id	Pixels	ROI Id	Pixels	ROI Id	Pixels	ROI Id	Pixels
	23	62	52	29	4	48	10	73	20	68	12	107
	19	19	50	20	13	37	15	34	14	67	19	30
	17	15	49	49	28	22	21	33	2	30	45	23
	35	15	48	9	29	22	11	26	5	24	18	22
	36	10	53	6	30	22	6	23	3	20	44	21
							34	23	42	17	37	17
							31	18	43	16	16	16
							25	17	1	13	40	15
							26	16	22	10	47	14
							32	16	38	10	39	12
							27	15			41	12
							7	14			46	11
							24	13			8	7
							33	13				
Total	5	121	5	81	5	151	14	334	10	275	13	307
Partial Total				29 ROIs – 687 Pixels						23 ROIs – 582 Pixels		
Grand Total	52 ROIs – 1269 Pixels											

This can greatly help differentiating plant signals from surrounding endmembers. Also, the pine species have needle-like leaves, which provide minimal leaf area index compared to broadleaf species. More branch and soil signals may be present due to the structure of the leaves.

3.1. Atmospheric Correction

Ground spectral measurements regarding atmospheric correction were collected concurrently with flight operations as mentioned in *OSBS Aero Measurements*. Unlike many other atmospheric correction algorithms that interpolate radiation transfer properties from a pre-calculated database of modeling results, FLAASH incorporates the MODTRAN radiation transfer code. Based on any of the standard MODTRAN model atmospheres and aerosol types specified, a unique MODTRAN solution is computed for each image. FLAASH (Elexis Inc.) also includes the following features: correction for pixel mixing due to scattering of surface-reflected radiance, compute a scene-average visibility (aerosol/haze amount), handling stressing atmospheric conditions (e.g. presence of clouds), cirrus and opaque cloud classification map, and adjustable spectral polishing for artifact suppression.

FLAASH starts from a standard equation for spectral radiance at a sensor pixel, L , that applies to the solar wavelength range (thermal emission is neglected) and flat, Lambertian materials or their equivalents. The equation is as follows [33]:

$$L_e \approx \left(\frac{(A + B)\rho_e}{1 - \rho_e S} + L_a \right) \quad (1)$$

where ρ_e is an *average* surface reflectance for the pixel and a surrounding region, S is the spherical albedo of the atmosphere, L_a is the radiance back scattered by the atmosphere, and A and B are coefficients that depend on atmospheric and geometric conditions but not on the surface. Solving for surface reflectance ρ_e , we have:

$$\rho_e \approx \frac{L_e - L_a}{A + B + S(L_e - L_a)} \quad (2-a)$$

ATCOR (ATCOR 4) has the following features: it can be combined with geometric information of terrain, a lookup table of a wide range of pre-calculated radiative transfer runs for different weather conditions and sun angles employing MODTRAN, incorporating spatially varying aerosol conditions, statistical haze removal that masks haze and cloud regions and removes haze of land areas, de-shadowing of cloud/building cast shadow areas, cirrus cloud removal, BRDF correction of irradiance effects, evaluation of atmospheric parameters (aerosol type, visibility, water vapor) by comparing retrieved reflectance with library spectra, adaption of solar reference spectrum. ATCOR performs atmospheric correction for surface reflectance ρ disregarding the adjacency component is as follows [39]:

$$\rho \approx \frac{\pi(d^2(c_0 + c_1 DN) - L_{path})}{\tau E_g} \quad (2-b)$$

where τ is the atmospheric (direct or beam) transmittance for a vertical path through the atmosphere, d is the earth-sun distance in astronomical units, c_0 , c_1 and DN are the radiometric calibration offset, gain, and recorded brightness (digital number), respectively; and E_g is the global flux on the ground.

3.1. Signal Pre-processing

We load hyperspectral images in Matlab using an in-house upgraded version of `enviread`, initially developed by Dr. Ian Howat at Ohio State University [40]. We check for the consistency of calibration and uniformity of pixel sizes and noticed a range of 3.3m to 3.6m pixel sizes due to various flight and measurement conditions. As different flights have different altitudes and hence pixel resolutions, this is an essential step to account for. Here we define a hyperspectral image I with dimensionality (x, y, w, z) , where $x \in X = [167000, 833000]$ represents the range of UTM Easting values, $y \in Y = [0, 9400000]$ represents UTM Northing values, $w \in W = \{1, \dots, 224\}$ is the index of the reflectance wavelengths, and $z \in Z = \{1, \dots, 60\}$ is the UTM zone of the image. Based on our observations, we take constant $\xi = 10000$ as a cut-off point to avoid erroneous sensor readings. There are some noises in JPL AVIRIS measurements such as negative reflectance values; the range of hyperspectral reflectance values is in range $[-32762, 32724]$: one should note that reflectance is the proportion of sun radiance signals which should be a positive value, but in normalized form reflectance is between zero and one. Below you can see the normalization process:

$$I_{xywz} = \begin{cases} 0 & \text{for } I_{xywz} < 0 \\ 1 & \text{for } I_{xywz} > \xi \\ \sqrt{\frac{I_{xywz}}{\xi}} & \text{otherwise} \end{cases} \quad (3)$$

To normalize we set negative reflectance values to zero and values greater than 10,000 to 10,000. To enhance the intensity of readings we take the square-root of signal returns. This procedure is due to

the following facts: a) There is no standard output of reflectance data and even reflectance of a single crown at different pixels can be quite different. Unlike minerals that have fixed and known reflectance values, trees can give different signal returns based on generation, number of leaf layers for the crown, leaf formation and orientation, leaf area index, condition of growth (water quality, climate, soil) and etc which can make this task challenging. b) Due to the resolution of images signals are all mixtures of several endmembers. Due to these reasons, empirically obtained thresholds and ranges are inevitable. Regarding square root, one should note that without taking the square root the images lack proper daylight intensity and appear dark. We exclude wavelengths corresponding to strong water vapor absorption bands in the atmosphere. This includes 1333.2 nm to 1482.7 nm, 1791.6 nm to 1967.4 nm, and 2406.9 nm to 2496.2 nm. Due to strong absorption at those wavelengths, the instrument measures a small radiance signal.

3.1.1. Impact of Non-vegetated/Shaded Pixels

A filter of $NIR < 0.33$ excludes heavily shaded samples which usually have distorted reflectance signals [1]. Normalized Difference Vegetation Index (NDVI) is an index which shows how green a pixel is and is usually used to remove material that does not belong to planetary material such as roads, clouds and any not-vegetated area, even grass and so on. NDVI is defined as below:

$$NDVI = \frac{NIR - VIS}{NIR + VIS} \quad (4)$$

where is NIR the reflectance in the reflective near-infrared wavelengths (725-1100 nm) and VIS is the reflectance in the visible (red) wavelengths (580-680 nm). The principle behind this is that VIS is in a part of the spectrum where chlorophyll causes considerable absorption of incoming radiation, and the NIR is in a spectral region where spongy mesophyll leaf structure leads to considerable reflectance [41,42]. For this purpose we chose the band at 665.6 nm for red and 734.1 nm for near-infrared. By filtering out pixels with $NDVI < 0.4$ we are essentially removing pixels that are not green. By properly applying an NDVI filter globally to a whole flight line, you will end up with major tree crowns. However, in our scenario we observed that preserving low NDVI/NIR pixels from ground data actually helps prediction accuracy. As you can see in Table 1, we have tens of pixels per ROI and considering that each pixel is about 3m wide and the fact that species of this study do not have wide crowns; this means that ROIs are generously marked and span across several neighboring tree crowns. This includes the empty spaces between crowns, shady pixels, understory grass, and etc. The initial expectation is that to properly classify tree species we should get rid of low NDVI pixels from such large canopies. Contrary to this belief due to the mixing nature of hyperspectral pixels and aggregate operation of classification techniques in multi-dimensional space, removing low NDVI pixels from *tree canopies* degraded classification performance by about 10%. So it is better to preserve low NDVI pixels in this scenario as they are mixed in with actual green pixels of trees and provide added value in the aggregate operation of SVM.

2.1.2. Gaussian Filter

Real-life sensor measurements are far from perfect and there are many noisy readings along different bands. We take advantage of abundance of bands and exploit their local-aggregated information by applying a Gaussian filter. We take a Gaussian window w of size $N > 0$, the coefficients of the Gaussian window are computed as below:

$$w(n) = e^{-\frac{1}{2}(\alpha \frac{n}{N/2})^2} \quad (5)$$

where $-\frac{N-1}{2} \leq n \leq \frac{N-1}{2}$, and α is inversely proportional to the standard deviation (σ) of a Gaussian random variable ($\sigma = \frac{N}{2\alpha}$). Once we have Gaussian parameters we perform convolution to apply the smoothing factor. By convolving vectors $u \in R^m$ and $v \in R^n$, we will have vector $w \in R^{m+n-1}$ such that:

$$w(k) = \sum_j u(j)v(k-j+1) \quad (6)$$

3.2. Support Vector Machine

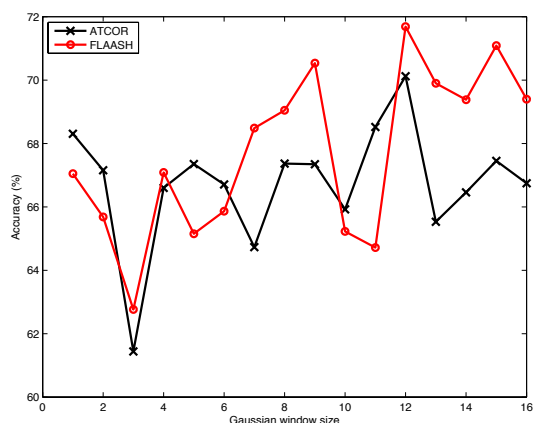
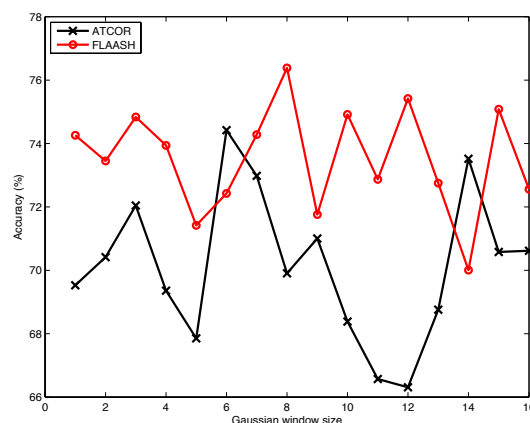
It is well known in literature that Support Vector Machine (SVM) outperforms other algorithms on species classification [1,13,43]. Our focus is on the impact of atmospheric correction (specifically FLAASH vs ATCOR) at pixel level classification using non-linear multi-class SVM. We parameterize SVM with k-fold cross validation where $k = 5$. Classifier non-linearity comes from taking the following non-linear functions as kernel for SVM:

- Polynomial function kernel.
- Radial Basis Function (RBF) kernel

Regarding multi-class classification, we create $\binom{c}{2}$ classifiers where c is the number of classes. In this case $c = 6$, hence we train 15 disjoint binary classifiers at each iteration of k-fold. We train all the classifiers and to decide on the class of a given test pixel, majority voting among classifiers decides which class it belongs to. We avoid aggregating classes of canopy pixels to determine the class of the whole canopy. This process can be performed using well known approaches such as majority of pixels, etc., which is not relevant to the purpose of this paper. Furthermore, the assumption that we always know the exact boundaries of all single-tree canopies does not always hold, specifically in dense vegetation, so we leave this out from our discussion.

4. Results and Discussion

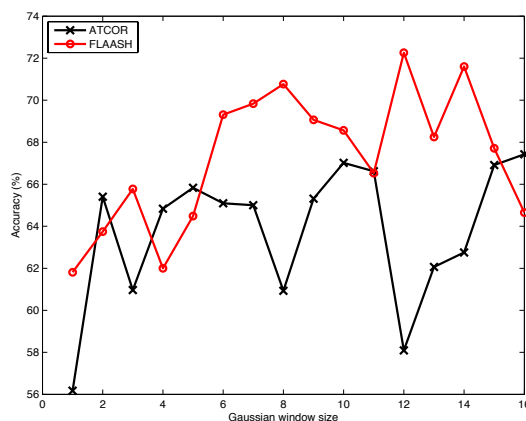
In this part we empirically evaluate the impact of optimizing classifier parameters regarding to FLAASH and ATCOR atmospheric corrections. As atmospheric correction is a low level signal processing technique, our focus is on the impact of data pre-processing filters on the performance of the species classification while we compare the two. An implementation of a one-vs-one multi-class k-fold cross-validation setup of SVM using non-linear kernels (polynomial and radial basis) functions is used for our model. Majority vote among classifiers determines the specie of a pixel. As for some of our species we only have at most 5 canopies and we cannot take $k > 5$ for a correct implementation of

Figure 4. Impact of Gaussian Filter on Prediction Accuracy.**(a)** Before removing water absorption bands.**(b)** After removing water absorption bands.

k-fold cross validation therefore we set $k = 5$. Test and train sets are canopy-aware, meaning that pixels of a single canopy are either used for training or test sets and not both. As pixels of one canopy can have many similarities, it is not suggested to use several pixels of a canopy for train and other pixels of the same canopy for test purposes. This could have the same meaning as using the same data both for train and test, which leads to over fitting and erroneous accuracy results. A mixture of grid search and heuristic optimization determines various parameters for SVM kernels, but for brevity we only present 2D diagrams here as other parameters settings are out of scope of this project. Specifically we set a cost of $C = \infty$ for misclassification, meaning that we have little to zero tolerance for improperly classified samples.

In Figure 4 we show how removing water absorption bands helps us improve prediction accuracy. Before removing these bands (Figure 4.a) prediction accuracy starts at about 66% and rises to about 71% as we increase Gaussian window size (about 5% performance improvement). There is a positive trend across different window sizes, which means we can expect better accuracy the bigger the window size gets. This stems from the fact that water absorption bands add to randomness and as we increase window size this randomness is dissolved to the majority of neighbors and would have less and less impact as window size increases. After removing water absorption bands (Figure 4.b) prediction accuracy starts at 74% and rises to about 76.5% at a window size of 8. Beyond that there is no significant change in accuracy. As window size increases you can see that there is no predictable impact of Gaussian smoothing in accuracy; This is due to the fact that all the currently available data signals has some level of inherent entropy (less noisy) and increasing window size beyond certain point just takes data away from their original meaning which can either help or harm accuracy in unpredictable ways. Before removing water absorption bands FLAASH shows minor advantages over ATCOR, but after removal this difference becomes a meaningful 4% better prediction accuracy for FLAASH.

Next, we look at the impact of removing low NDVI-NIR pixels from dataset. As you can see in Figure 5 there is a general degradation of performance from the previous scenario that we used the whole dataset. In FLASSH dataset we are at about 70% and ATCOR yields 66% accuracy. This is due to the fact that pixel size is large (3m) and canopies are large as well. According to Table 1, canopy sizes are in the range of [6,107] pixels. This generous marking of canopies includes areas with little

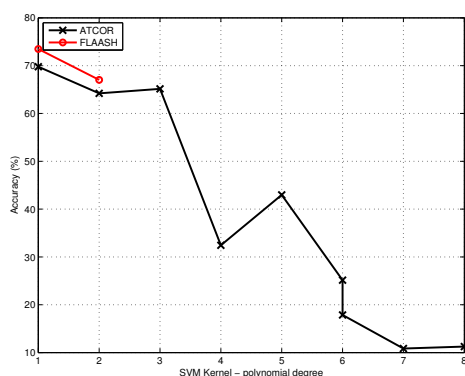
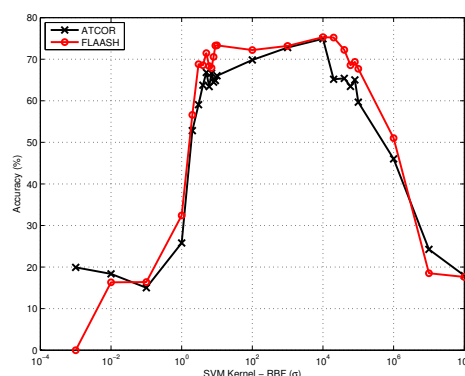
Figure 5. Impact of removing low NDVI and NIR pixels among field data

greenness, shadows, branches, gravel and etc (all with low NDVI and low NIR values). But you should note that due to the mixing nature of reflectance values, even low NDVI/NIR pixels of a continuous canopy, still contains signals from the underlying species, which might not be as green. Here we can see that removing low NDVI/NIR pixels of a continuous canopy actually degrades the performance of the classification model with an impact of about 4%. So in similar scenarios where *field data* consists of large continuous canopies we advise on preserving low NDVI/NIR pixels. It is important to realize that this is only relevant in the context of field data, as we already know the species are there, and is only useful in training the classifier. In global application of NDVI/NIR filters to whole flight lines we suggest as literature does which is removal of low values to get rid of roads, grass, etc. Here we can still observe the benefit of FLAASH data versus ATCOR on average by 2%-3%.

Finally, we look at the effect of atmospheric correction on prediction accuracy vs classification model parameters. C , σ , P , MaxIter and *optimization method* are the knobs of SVM that we tune in a mixture of grid and heuristic search. C stands for cost or penalty of misclassification against simplicity of the decision surface, σ (or also known as γ in literature) defines how far the influence of a single training example reaches, with low values meaning 'far' and high values meaning 'close' in RBF function. P is the polynomial degree for polynomial function as kernel. MaxIter is the maximum number of iterations the optimization function is supposed to run; and *optimization method* defines what optimization method we select. Here we set $C=+\infty$, MaxIter=10,000 and use quadratic programming as *optimization method*. In what follows we evaluate the impact of P and σ respectively as demonstrated in Figure 6.

Figure 6.a demonstrates the impact of polynomial degree P on prediction accuracy using a polynomial kernel in SVM. FLAASH atmospherically corrected data yields 73.5% of accuracy whereas ATCOR results in 69.8%. The simpler the polynomial, the better the performance; with a more complicated polynomial we get a high bias classification model which performs poorly when evaluated on test data. For FLAASH atmospheric correction ($P \geq 3$) the optimization function does not converge. On the other hand, ATCOR data performs as predicted. Accuracy gets as low as 10.8% and 11.3% with polynomial degrees of 7 and 8 (due to extreme over-fitting).

The Radial Basis kernel has better performance yields than polynomial. As shown in Figure 6.b, with a peak at 75.3% we achieve the best results using FLAASH data while ATCOR comes close at 74.9%. RBF does not show good performance at either too low or too high σ values. σ is the inverse of

Figure 6. Parameter tuning for classification algorithms.**(a)** Tuning P for SVM with polynomial kernel function.**(b)** Tuning σ in SVM with RBF kernel function.

the width of the RBF kernel (roughly defining the area of influence of a support vector); in other terms, it defines how much influence a single training example has. The larger σ is, the closer other examples must be to be affected. As RBF takes data to a higher dimensionality a small σ gives you a pointed bump in the higher dimensions, and a large σ gives you a softer, broader bump. So neither extreme shows a good fit and a middle point of $\sigma = 10,000$ provides best results. On the negative side, FLAASH begins with an accuracy of 0% and ATCOR at 19.9%, but they quickly get to a stable region close by to each other while FLAASH demonstrates superior performance in most of the cases. There is a good range of σ values ([10, 10000]) where we reach a plateau in prediction accuracy, which implies a more robust performance than polynomial.

Table 2 demonstrates the confusion matrix of the proposed classification model at a near peak setup (75.2%). You can see that the majority of misclassifications are between Pine (other) class and Longleaf Pine. Similar misclassification can be found between Oak (other) and other types of Oak. This is due to the fact that this class of Oak or Pines is a mixture of different types of Oak or Pine respectively, which might include Longleaf Pine or Laurel Oak and such conformance might be unavoidable. The main advantage of this experiment is that there is mere misclassification between oak vs. pine category. The oak category is rarely misclassified as pine, but pines have been mistaken with Turkey Oak and Laurel Oak. One should also note that different species of oak are not misclassified to each other. Laurel Oak, Turkey Oak and Live Oak are well separable from each other, and this shows a good intra broad-leaf species classification.

Table 2. Confusion Matrix for Species Classification

	Predicted Class						Sum
	Pine (other)	Longleaf Pine	Turkey Oak	Live Oak	Oak (other)	Laurel Oak	
Known Class	Pine (other)	10	10	3	0	0	23
	Longleaf Pine	20	36	0	0	4	60
	Turkey Oak	1	0	62	0	0	63
	Live Oak	0	0	44	4	0	48
	Oak (other)	0	0	0	0	9	10
	Laurel Oak	1	0	0	0	5	6
	Sum	32	46	65	44	18	210

In our experiments we observed better performance of FLAASH atmospherically corrected data versus ATCOR. This is in conformance with recent observations of Manakos et. al. [35] where they focused on basic endmember classification (asphalt, gravel, rocky areas, reddish soil, agricultural areas, grass/dry grass, mequis, and phrygana) but we look into the actual problem of tree species classification.

5. Conclusions

Identifying species using remote sensing technologies such as hyperspectral and LiDAR sensors has a critical utility in studying global warming, bio-mass estimation, carbon preserves, invasive species identification and etc. In this paper we perform species classification using SVM over AVIRIS hyperspectral data available for Ordway Swisher Biological Station in north-central Florida. Our focus is on comparing FLAASH and ATCOR atmospheric corrections while we propose using Gaussian filter for de-noising reflectance values. We also discuss how incorporating even low NDVI and low NIR pixels can be helpful in improving classification accuracy in large canopy areas. Due to the mixing nature of remote sensing hyperspectral data, using such pixels can reduce the bias in maximum margin support vectors in SVM. Our observation shows a clear advantage on using FLAASH vs. ATCOR, by margins of about 2% to 4%. Our classification model is robust for intra oak species classification; with minor inter conifer/broad-leaf misclassified labels.

Acknowledgments

Authors are thankful to NEON Inc. for providing hyperspectral data. Also they are thankful to Ms. Sarah Graves, Ms. Leila Kalantari and Dr. Stephanie Bohlman for providing field data. The National Ecological Observatory Network is a project sponsored by the National Science Foundation and managed under cooperative agreement by NEON, Inc. The NEON 2010 Pathfinder data set is based on work supported by the National Science Foundation under Grant DBI-0752017.

References

1. Colgan, M.S.; Baldeck, C.A.; Féret, J.-B.; Asner, G.P. Mapping savanna tree species at ecosystem scales using support vector machine classification and brdf correction on airborne hyperspectral and lidar data. *Remote Sensing* **2012**, *4*, 3462-3480.
2. Scholes, R.; Archer, S. Tree-grass interactions in savannas. *Annual review of Ecology and Systematics* **1997**, *28*, 517-544.
3. Féret, J.-B.; Asner, G.P. Tree species discrimination in tropical forests using airborne imaging spectroscopy. *Geoscience and Remote Sensing, IEEE Transactions on* **2013**, *51*, 73-84.
4. Dalponte, M.; Ørka, H.O.; Ene, L.T.; Gobakken, T.; Næsset, E. Tree crown delineation and tree species classification in boreal forests using hyperspectral and als data. *Remote sensing of environment* **2014**, *140*, 306-317.
5. Féret, J.-B.; Asner, G.P. Semi-supervised methods to identify individual crowns of lowland tropical canopy species using imaging spectroscopy and lidar. *Remote Sensing* **2012**, *4*, 2457-2476.
6. Ghosh, A.; Fassnacht, F.E.; Joshi, P.; Koch, B. A framework for mapping tree species combining hyperspectral and lidar data: Role of selected classifiers and sensor across three spatial scales. *International Journal of Applied Earth Observation and Geoinformation* **2014**, *26*, 49-63.

7. Immitzer, M.; Atzberger, C.; Koukal, T. Tree species classification with random forest using very high spatial resolution 8-band worldview-2 satellite data. *Remote Sensing* **2012**, *4*, 2661-2693.
8. Naidoo, L.; Cho, M.; Mathieu, R.; Asner, G. Classification of savanna tree species, in the greater kruger national park region, by integrating hyperspectral and lidar data in a random forest data mining environment. *ISPRS Journal of Photogrammetry and Remote Sensing* **2012**, *69*, 167-179.
9. Ustin, S.L.; Gitelson, A.A.; Jacquemoud, S.e., phane; Schaepman, M.; Asner, G.P.; Gamon, J.A.; Zarco-Tejada, P. Retrieval of foliar information about plant pigment systems from high resolution spectroscopy. *Remote Sensing of Environment* **2009**, *113*, S67-S77.
10. Clark, M.L.; Roberts, D.A.; Clark, D.B. Hyperspectral discrimination of tropical rain forest tree species at leaf to crown scales. *Remote sensing of environment* **2005**, *96*, 375-398.
11. Clark, M.L.; Roberts, D.A. Species-level differences in hyperspectral metrics among tropical rainforest trees as determined by a tree-based classifier. *Remote Sensing* **2012**, *4*, 1820-1855.
12. Baldeck, C.A.; Asner, G.P. Estimating vegetation beta diversity from airborne imaging spectroscopy and unsupervised clustering. *Remote Sensing* **2013**, *5*, 2057-2071.
13. Baldeck, C.; Colgan, M.; Féret, J.-B.; Levick, S.; Martin, R.; Asner, G. Landscape-scale variation in plant community composition of an african savanna from airborne species mapping. *Ecological Applications* **2014**, *24*, 84-93.
14. Green, A.A.; Berman, M.; Switzer, P.; Craig, M.D. A transformation for ordering multispectral data in terms of image quality with implications for noise removal. *Geoscience and Remote Sensing, IEEE Transactions on* **1988**, *26*, 65-74.
15. Liang, S.; Fang, H.; Chen, M. Atmospheric correction of landsat etm+ land surface imagery. I. Methods. *Geoscience and Remote Sensing, IEEE Transactions on* **2001**, *39*, 2490-2498.
16. Ouaidrari, H.; Vermote, E.F. Operational atmospheric correction of landsat tm data. *Remote Sensing of Environment* **1999**, *70*, 4-15.
17. Ju, J.; Roy, D.P.; Vermote, E.; Masek, J.; Kovalsky, V. Continental-scale validation of modis-based and ledaps landsat etm+ atmospheric correction methods. *Remote Sensing of Environment* **2012**, *122*, 175-184.
18. Gao, B.-C.; Montes, M.J.; Davis, C.O.; Goetz, A.F. Atmospheric correction algorithms for hyperspectral remote sensing data of land and ocean. *Remote Sensing of Environment* **2009**, *113*, S17-S24.
19. Janzen, D.T.; Fredeen, A.L.; Wheate, R.D. Radiometric correction techniques and accuracy assessment for landsat tm data in remote forested regions. *Canadian Journal of Remote Sensing* **2006**, *32*, 330-340.
20. Watmough, G.R.; Atkinson, P.M.; Hutton, C.W. A combined spectral and object-based approach to transparent cloud removal in an operational setting for landsat etm+. *International Journal of Applied Earth Observation and Geoinformation* **2011**, *13*, 220-227.
21. Wu, J.; Wang, D.; Bauer, M.E. Image-based atmospheric correction of quickbird imagery of minnesota cropland. *Remote Sensing of Environment* **2005**, *99*, 315-325.
22. Vaudour, E.; Moeys, J.; Gilliot, J.; Coquet, Y. Spatial retrieval of soil reflectance from spot multispectral data using the empirical line method. *International Journal of Remote Sensing* **2008**, *29*, 5571-5584.
23. Xu, J.-F.; Huang, J.-F. Empirical line method using spectrally stable targets to calibrate ikonos imagery. *Pedosphere* **2008**, *18*, 124-130.
24. Hadjimitsis, D.G.; Papadavid, G.; Agapiou, A.; Themistocleous, K.; Hadjimitsis, M.; Retalis, A.; Michaelides, S.; Chrysoulakis, N.; Toullos, L.; Clayton, C. Atmospheric correction for satellite remotely sensed data intended for agricultural applications: Impact on vegetation indices. *Natural Hazards and Earth System Science* **2010**, *10*, 89-95.

25. Manakos, I.; Liebler, J.; Schneider, T. Parcel based calibration of remote sensing data for precision farming purposes. *Proceedings: Angewandte Geographische Informationsverarbeitung XII* **2000**, 333-344.
26. Hadjimitsis, D.G.; Clayton, C.; Retalis, A. The use of selected pseudo-invariant targets for the application of atmospheric correction in multi-temporal studies using satellite remotely sensed imagery. *International Journal of Applied Earth Observation and Geoinformation* **2009**, *11*, 192-200.
27. Kotchenova, S.Y.; Vermote, E.F.; Matarrese, R.; Klemm Jr, F.J. Validation of a vector version of the 6s radiative transfer code for atmospheric correction of satellite data. Part i: Path radiance. *Applied optics* **2006**, *45*, 6762-6774.
28. Berk, A.; Anderson, G.P.; Bernstein, L.S.; Acharya, P.K.; Dothe, H.; Matthew, M.W.; Adler-Golden, S.M.; Chetwynd Jr, J.H.; Richtsmeier, S.C.; Pukall, B. In *Modtran4 radiative transfer modeling for atmospheric correction*, SPIE's International Symposium on Optical Science, Engineering, and Instrumentation, 1999; International Society for Optics and Photonics: pp 348-353.
29. Richter, R. In *Atmospheric correction of dais hyperspectral image data*, Aerospace/Defense Sensing and Controls, 1996; International Society for Optics and Photonics: pp 390-399.
30. Richter, R. Correction of satellite imagery over mountainous terrain. *Applied Optics* **1998**, *37*, 4004-4015.
31. Richter, R.; Schläpfer, D. Geo-atmospheric processing of airborne imaging spectrometry data. Part 2: Atmospheric/topographic correction. *International Journal of Remote Sensing* **2002**, *23*, 2631-2649.
32. Richter, R.; Schläpfer, D. Atmospheric/topographic correction for satellite imagery. *DLR report DLR-IB* **2005**, 565-501.
33. Adler-Golden, S.M.; Matthew, M.W.; Bernstein, L.S.; Levine, R.Y.; Berk, A.; Richtsmeier, S.C.; Acharya, P.K.; Anderson, G.P.; Felde, J.W.; Gardner, J., *et al.* In *Atmospheric correction for shortwave spectral imagery based on modtran4*, SPIE's International Symposium on Optical Science, Engineering, and Instrumentation, 1999; pp 61-69.
34. Adler-Golden, S.; Berk, A.; Bernstein, L.; Richtsmeier, S.; Acharya, P.; Matthew, M.; Anderson, G.; Allred, C.; Jeong, L.; Chetwynd, J. In *Flaash, a modtran4 atmospheric correction package for hyperspectral data retrievals and simulations*, Proc. 7th Ann. JPL Airborne Earth Science Workshop, 1998; pp 97-21.
35. Manakos, I.; Manevski, K.; Kalaitzidis, C.; Edler, D. In *Comparison between atmospheric correction modules on the basis of worldview-2 imagery and in situ spectroradiometric measurements*, 7th EARSeL SIG Imaging Spectroscopy workshop, Edinburgh, 2011; pp 11-13.
36. Kampe, T.U.; Johnson, B.R.; Kuester, M.; Keller, M. Neon: The first continental-scale ecological observatory with airborne remote sensing of vegetation canopy biochemistry and structure. *Journal of Applied Remote Sensing* **2010**, *4*, 043510-043510.
37. Krause, K.; Kuester, M. Airborne observation platform (aop) pathfinder 2010 data release. <http://neoninc.org/pds/files/NEON.AOP.015068.pdf>.
38. Kampe, T.; Krause, K.; Meiera, C.; Barnetta, D.; McCorkela, J. The neon 2010 airborne pathfinder campaign in florida. 2010.
39. Richter, J.; Schläpfer, D. In *Atmospheric / topographic correction for satellite imagery*, ATCOR-2/3 User Guide, Version 8.3.1, February 2014, 2014.
40. Howat, I. Envi file reader, updated 2/9/2010. <http://www.mathworks.com/matlabcentral/fileexchange/15629-envi-file-reader--updated-2-9-2010>.
41. Tucker, C.J. Red and photographic infrared linear combinations for monitoring vegetation. *Remote sensing of Environment* **1979**, *8*, 127-150.

42. Jackson, R.; Slater, P.; Pinter Jr, P. Discrimination of growth and water stress in wheat by various vegetation indices through clear and turbid atmospheres. *Remote sensing of environment* **1983**, *13*, 187-208.
43. Cho, M.A.; Mathieu, R.; Asner, G.P.; Naidoo, L.; van Aardt, J.; Ramoelo, A.; Debba, P.; Wessels, K.; Main, R.; Smit, I.P., *et al.* Mapping tree species composition in south african savannas using an integrated airborne spectral and lidar system. *Remote Sensing of Environment* **2012**, *125*, 214-226.

© 2015 by the authors; licensee MDPI, Basel, Switzerland. This article is an open access article distributed under the terms and conditions of the Creative Commons Attribution license (<http://creativecommons.org/licenses/by/4.0/>).